氏　　名	何　　楽　年
生年月日	
本　　籍	中国
学位の種類	博士（工学）
学位記番号	博甲第163号
学位授与の日付	平成８年３月25日
学位授与の要件	課程博士（学位規則第４条第１項）
学位授与の題目	Microscopic structure of silicon-based amorphous dielectrics （Si系アモルファス絶縁膜における微視的結合構造）
論文審査委員	(主査)　長谷川　誠一 (副査)　清水立生，畑　朋延 久米田　稔，森本章治

学位論文要旨

Shifts of the Si $2p$, O $1s$ and N $1s$ core-level spectra with the O and N content x for a-SiO_x and a-SiN_x films were examined by means of the charge-transfer model (CTM) model, in which the average partial charge on a given atom is expressed as a function of x, by using Sanderson's electronegativity results and the random-bonding model (RBM). The CTM model reveals that spacing of the Si $2p$ lines due to five $Si(Si_{4-n}M_n)$ (M = O or N) bonding units based on the RBM decreases with increasing n. Moreover, the CTM is also useful to derive the peak frequencies of the Si–H and Si–O stretching absorption bands in a-SiO_x:H films. Comparing the Si–H and Si–O bending absorption bands with Si–H stretching absorption bands, it was found that the intensities of the 780, 840 and 880 cm^{-1} bands are closely corrected with those of 2115, 2200 and 2260 cm^{-1} bands, respectively. For a-SiO_x films, the anisotropic g factors due to Si dangling bond centers with $\cdot Si{\equiv}SiO_2$ and $\cdot Si{\equiv}O_3$ configurations were determined by a curve-fitting analysis, and compared with results of a molecular orbital calculation. From the behaviors of stress in a-SiO_2 films, it was found there are close relationships among the stress, the Si–O stretching absorption band, the buffered HF etch rate, the density of Si dangling bonds and the deposition rate. Based on the compositional analysis of a-SiO_xN_y:H films, we found that very low concentration of homobonds, such as Si-Si, O-O, N-N, and of Si-H and O-H bonds are incorporated in the films. The results of IR absorption measurements reveal that the chemical structure of a-SiO_xN_y:H films is homogeneous.

Chapter 1. Introduction

Silicon-based amorphous dielectrics such as a-SiN_x:H, a-SiO_x:H and a-SiO_xN_y:H films are widely used in a variety of electronic devices as antireflective coating layers in solar cells, as gate insulators in metal-insulator-semiconductor devices and as passivation layers. The electronic, optical and mechanical properties of the films are often linked inextricably to the films structure, therefore, it is necessary to understand the bonding configurations of films. Moreover, it is extremely important to explore the origin and structure of the defects, and to understand the characteristics of mechanical stress in the films. Although considerable progress has been made in accounting for the chemical structure and electronic and optical properties of a-Si-based dielectrics, some of basic aspects remain relatively

poor understood, such as partial charge on Si, O and N atoms for a-SiO_x and a-SiN_x films, and the local vibrational properties of a-SiO_x:H films, *etc.* The purpose of this research is to make efforts to understanding the microscopic structure of a-SiO_x:H, a-SiN_x:H and a-SiO_xN_y:H films, prepared by plasma-enhanced vapor deposition (PECVD) methods.

Chapter 2. Analysis of photoemission in amorphous SiO_x and SiN_x alloys in terms of a charge-transfer model

In order to analyse the shift of Si $2p$, O $1s$ and N $1s$ core-level spectra with the O and N content x for a-SiO_x and a-SiN_x films, we have considered an charge-transfer model (CTM). In the CTM, the partial charge on a given atom, $P_M(x)$ (M = Si, O or N), which dominates the X-ray photoelectron spectra, were calculated by means of Sanderson's electronegative results and random-bonding model (RBM). Moreover, charge neutrality in a given atomic species was examined. Figure 1 shows effective peak binding energy, E_B(Si $2p$) of Si $2p$ as a function of the averaged partial charge, $P_{Si}(x)$ on a Si atom per single bond in a-SiO_x, a-SiN_x and stoichiometric SiC, Si_3N_4 and SiO_2 films. The E_B(Si $2p$) for all kinds of samples are found to be linearly related to $P_{Si}(x)$ with a relation of

$$E_B(\text{Si } 2p) = 10.2P_{Si}(x) + 99.3. \qquad (1)$$

The Eq. (1) predicts that addition of a unit of positive charge onto a Si atom shifts E_B(Si $2p$) towards higher binding energy by 2.55 eV. In Fig. 1, the deviation of the data from the straight line for a-SiO_x and a-SiN_x occurring at x above 1.2 and 0.7, respectively, is probably due to a charging effect during the XPS measurement. Furthermore, the CTM model showed that spacing of the Si $2p$ line arising from each of five Si($Si_{4-n}M_n$) (n = 0,1,...4; M = O or N) bonding units based on the RBM decreases with increase n

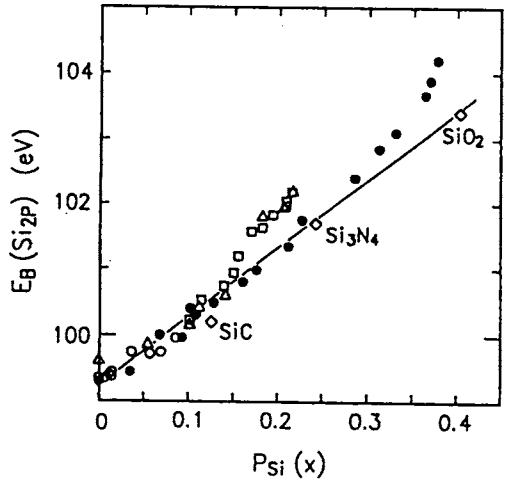

Fig. 1. Effective peak binding energy, E_B(Si $2p$), of the Si $2p$ as a function of the averaged partial charge, $P_{Si}(x)$, on a Si atom per single bond in a-SiO_x (close circles), a-SiN_x films (open circles, triangles and squares), and those for stoichiometric films, SiC 25-Å-thick Si_3N_4, and SiO_2, are shown for comparison.

Chapter 3. Vibrational properties of Si–O and Si–H in amorphous SiO_x:H films

The stretching and banding vibration modes of Si–H and Si–O bonds in a-SiO_x:H films were investigated by means of infrared (IR) absorption measurements as a function of O content x. Figure 2 shows the IR absorption profiles of the Si–H stretching mode and the result of a curve fitting analysis over 1800–2500 cm^{-1} range for films with three different compositions of x = 0.16, 0.92 and 2.0. The observed profiles of the Si–H stretching absorption can be decomposed into four components at around 2000, 2115, 2200 and 2260 cm^{-1}. On the basis

of a modified random-bonding (MRB) model, incorporation of Si–H bonds into the films can be performed by replacing one of Si nearest neighbors at the Si site in $Si(Si_{4-n}O_n)$ (n = 0–3) configurations by a H atom. Thus, the 2000, 2115, 2200 and 2260 cm^{-1} bands are assigned with $H\text{–}Si(Si_{3-n}O_n)$ configurations for n = 0, 1, 2 and 3, respectively. On the other hand, the peak frequencies of the Si–H absorption bands, arising from $H\text{–}Si(Si_2O)$ and $H\text{–}Si(SiO_2)$ bonds, were calculated using the CTM, and found to be 2110 and 2194 cm^{-1}. These results agree well with those determined through a curve-fitting method.

The absorption spectra over the 600 to 900 cm^{-1} range were also investigated by the curve-fitting method. Five components at around 650, 780, 800, 840 and 880 cm^{-1} can be decomposed. These bands are associated with either Si–H or Si–O–Si bending modes. The absorption intensities of the 780, 840 and 880 cm^{-1} bands, for films obtained as a function of x, display their respective good linear relationships with those of the Si–H stretching bands at around 2115, 2200 and 2260 cm^{-1}. This result indicates that the origins for each group of the 780 and 2115 cm^{-1} bands, the 840 and 2200 cm^{-1} bands, and the 880 and 2260 cm^{-1} bands are attributed to $H\text{–}Si(Si_2O)$, $H\text{–}Si(SiO_2)$ and $H\text{–}Si(O_3)$ configurations, respectively.

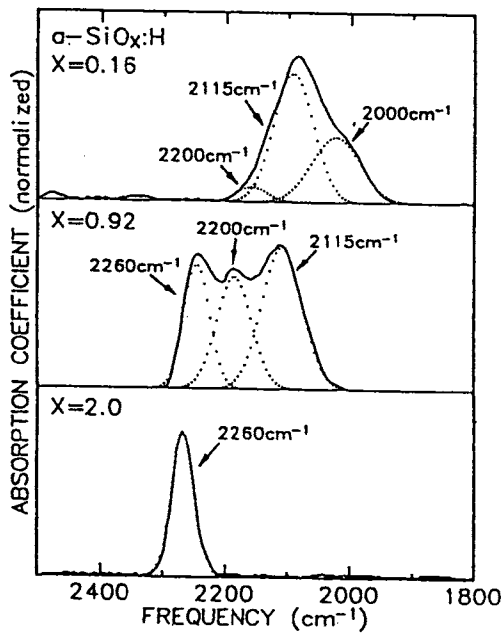

Fig. 2. Vibrational spectra over the 1800 to 2500 cm^{-1} range for a-SiO_x:H films with the x values of 0.16, 0.92 and 2.0. The broken lines are the results of a curve-fitting analysis.

Chapter 4. Electron spin resonance spectra of silicon dangling bonds with oxygen back bonds in amorphous SiO_x films

On order to explore the origin and structure of the defects in a-SiO_x films, we have studied the ESR spectra in a-SiO_x films as a function of x. For $x < 1.5$, a broad resonance line similar to the spectrum for a-Si:H dominates the ESR spectra, and which was attributed to Si dangling bond centers with a $\cdot Si{\equiv}Si_3$ configuration. The narrow lines, which became pronounced over the broad line for $x > 1.5$, were assigned to the signal arising from Si dangling bond centers with $\cdot Si{\equiv}Si_2O$, $\cdot Si{\equiv}SiO_2$, and $\cdot Si{\equiv}O_3$ configurations.

Figure 3 shows typical results of simulated spectra on experimental ones. In the simulated analysis, we took into account the anisotropy of g factors for $\cdot Si{\equiv}Si_{3-n}O_n$ (n = 1–3) centers, and used a powder pattern to describe the resonance intensity for a given value g. We can see a good agreement between the experimental and the fitted lines. Furthermore, the values of g factors determined by the curve-fitting analysis were found to be qualitative agreement with results of a molecular orbital calculation. A decrease in broadening factor of ESR lines for $\cdot Si{\equiv}Si_{3-n}O_n$ with increasing n, suggests that the structural fluctuation in the vicinity of the Si dangling bonds is reduced by the presence of an O back bond.

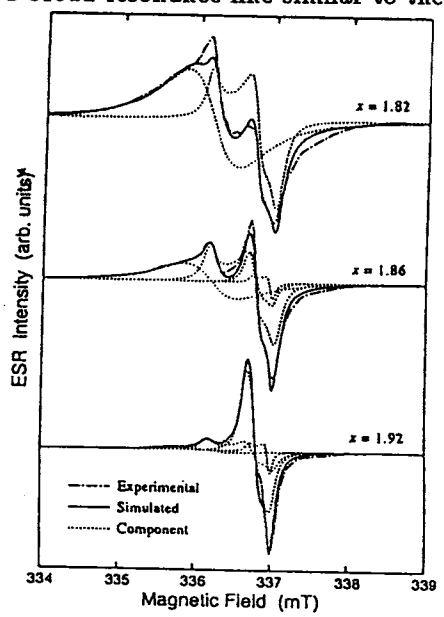

Fig. 3. Typical results of the fitting of the simulated spectra on experimental ones.

Chapter 5. Stress in amorphous SiO_x films

The dependence of stress on the O content x in a-SiO_x films was investigated. For stoichiometric a-SiO_2 films, changes in the stress and the bonding properties were investigated as functions of the

deposition time, the total flow rate of the feed gas and deposition temperature T_d. It was found that the stress and elastic constant $[Y/(1-\nu)]$ for a-SiO_x films strongly depend on x.

For a-SiO_2 films with $T_d < 300°C$, the stress is mainly caused by effects of the thermal expansion mismatch. The stress for a-SiO_2 films with $T_d \geq 300°C$ is dominated by the intrinsic stress. Table I shows the values of stress σ_Q and $Y/(1-\nu)$ for a-SiO_2 films having a deposition rate of 270–290 Å/min deposited at 100, 300 and 500°C and those for films having 560–600 Å/min at 100 and 300°C. It is found that the values of σ_Q and $Y/(1-\nu)$ for $T_d < 300°C$ strongly depend on T_d, while that these values for $T_d \geq 300°C$ are dominated by a change in the deposition rate rather than that in T_d. In addition, it is found that there are close relationships among the stress, the Si–O stretching absorption band, the buffered HF etch rate, the density of Si dangling bonds and the deposition rate.

Table I. Stress, σ_Q, observed for films deposited on the quartz substrates and elastic constant, $Y/(1-\nu)$, for a-SiO_2 films.

Sample	Total flow rate (sccm)	Deposition rate (Å/min)	T_d (°C)	σ_Q (10^8 N/m^2)	$Y/(1-\nu)$ (10^{10} N/m^2)
1A	2.7	290	100	−1.0	21
3A	2.8	270	300	0.33	8.4
5A	4.1	280	500	0.35	6.6
1B	4.1	600	100	−1.8	50
3B	4.8	560	300	−0.5	7.6

Chapter 6. Properties of "stoichiometric" silicon oxynitride films

The properties of amorphous silicon oxynitride (a-SiO_xN_y:H) films were investigated as functions of x and y. Figure 4 shows the dependence of x on y in a-SiO_xN_y:H films. The solid straight line in Fig. 4 is a results of a least-squares fit on the experimental data, and a relationship of $2x + 2.8y = 4$ is found. If the nearest neighbor of every Si site in the film is either an O or a N atom, the relationship between x and y should be expressed as $2x + 3y = 4$, which is represented by a broken line in Fig. 4, because the coordination numbers of O, N and Si are 2, 3 and 4, respectively. The reduction from 3.0 to 2.8 of the coefficient for the y in the linear function of Fig. 4 would be due to incorporation of N–H bonds. Thus, it suggests the densities of homobonds such as Si–Si, O–O and N–N, and of Si–H and O–H bonds are sufficiently lower than those of Si–O and Si–N bonds.

The properties of dangling bonds in a-SiO_xN_y:H films and their origins were discussed. As a result, it was suggested that creation of N-related dangling bonds would be enhanced by increasing O content in nitride films.

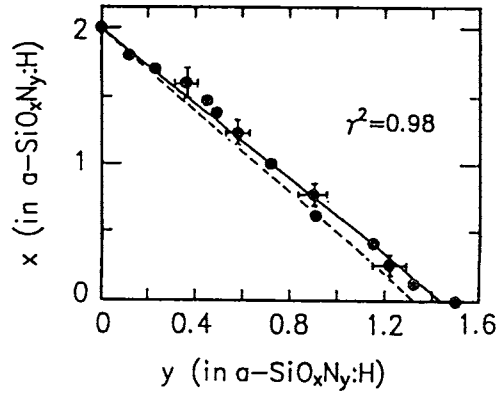

Fig. 4. Dependence of the oxygen content x as a function of the N content y in a-SiO_xN_y:H. The solid line in the figure is the result of a least-squares fit on the experimental data. The broken line expresses the relationship of $2x + 3y = 4$.

Chapter 7. Concluding summary

1) The Si $2p$ binding energy was found to be linear related to the averaged partial charge.

2) It suggests that the Si $2p$ line arising from each of five $Si(Si_{4-n}M_n)$ (n = 0,1,...4; M = O or N) bonding units decreases with increasing n.

3) The peak frequencies of the Si–H and Si–O stretching absorption bands in a-SiO_x:H films were calculated using the CTM. The calculated frequencies are in excellent agreement with the experimental results.

4) The 780, 800, 840 and 880 cm^{-1} bands are suggested to be related with H–Si(Si_2O), Si(O_4), H–Si(SiO_2) and H–Si(O_3) configurations, respectively.

5) The anisotropic g factors for the ·Si≡Si_2O and ·Si≡SiO_2 centers determined by a curve-fitting analysis were found to be qualitative agreement with results of a molecular orbital calculation.

6) For a-SiO_2 films with deposition temperature $T_d < 300°C$, the stress is mainly caused by effects of the thermal expansion mismatch. The stress for a-SiO_2 films with $T_d \geq 300°C$ is dominated by the intrinsic stress.

7) Amorphous SiO_xN_y:H films with very low concentration of homobonds such as Si–Si, O–O, N–N, and of Si–H and O–H bonds were obtained by PECVD methods under proper deposition conditions.

学位論文の審査結果の要旨

各審査委員が提出論文の審査を行い，さらに平成８年２月１日の口頭発表の後，その結果を踏まえて論文審査会を開催し協議の結果次の通り判定した。

本論文で取り扱う，プラズマ CVD 法による Si 酸化膜，Si 窒化膜および Si 酸化窒化膜は，薄膜トランジスタにおけるゲート絶縁膜や，最終保護膜，集積回路素子における層間絶縁膜として利用されている。本論文では，堆積条件（組成比や堆積温度など）の変化に伴う，電気的および光学的，機械的性質に強く影響する微視的な結合構造の変化，および膜中の欠陥構造の変化を系統的に調べ，その原因を明らかにしている。

提示された主な結果は，*i*）ランダムボンディングモデル及びサンダーソンの電気陰性度による解析法を用いて，膜中の構成 Si, O, N 原子上の平均部分電荷量を組成の関数として求めることができることを示した。その結果は，組成変化に伴う，Si *2p*, O *1s*, N *1s* コア電子の結合エネルギーの変化を良く説明した。*ii*）Si 酸化膜における Si-H および Si-O 結合から生ずる赤外吸収信号，Si ダングリングボンドに起因する ESR 信号，および膜中応力の組成による変化を調べ，微視的構造変化と関連づけて検討した。*iii*）「化学量論組成」をもつ Si 酸化窒化膜について，O および N 量の変化による誘電特性および結合構造の変化を調べると共に，欠陥の種類およびその発生機構の変化と関連づけた。

以上の結果は，今後の Si 系誘電体薄膜の応用に関する研究分野に極めて有用な指針を与えるものである。従って，本論文は博士（工学）の学位に値するものと判定する。